Chapter 1

Implications Of Considering Transport Type In Vapor Intrusion Investigations

1.1 Summary

Summary of stuff

1.2 Advective Transport: Considering Soil And Foundation Type

The modeling in Chapter **??** help explain why building pressurization was much more strongly associated before the closing of the preferential pathway. The preferential pathway lead to advective transport to be the dominant transport mechanism for entry of contaminant vapors through the foundation crack. This finding has wider implications on our understanding of the entry mechanics of VI.

It is commonly assumed that advective transport dominates in the near-foundation region and through breaches in the foundation itself, but our modeling shows that this was only possible because:

1. The preferential pathway supplied a source from where air could readily be drawn.

2. The permeable gravel sub-base acted as a communication medium between the preferential air source and the building.

In other words, for advective transport to dominate through foundation cracks, some site-specific features were required, and the soil itself presents too much resistance to air flow for this to be possible.

Only one soil type was explored in the modeling work in Chapter **??** - sandy clay, which is itself a relatively impermeable soil, and other soil type should be considered. Furthermore, our modeled house featured a basement, and in such a scenario, the atmosphere is relatively far removed from the foundation crack, and therefore, a slab-on-grade type of foundation should also be considered.

The effect of different soil and foundation types is investigated using the model introduced in Chapter **??**; the only difference is that we change the soil type and depth of the foundation. We consider 12 of the soil types studied by the EPA (see Table **??**) and for each of these we consider a basement and a slab-on-grade case respectively. The basement and slab-on-grade cases are defined by the bottom of foundation slab located at 1 m and 15 cm bgs respectively. To building is assumed to be depressurized at $p_{in} = -15\,\mathrm{Pa}$, a value much greater than "normal", to enhance the advective potential. The analysis in Chapter **??** showed that a gravel sub-base layer, absent a preferential air source, was virtually indistinguishable from the cases where there was no gravel sub-base layer, thus such a feature will not be included in the model.

The result of these model cases can be seen in Figure 1.1. This shows that for most soil types, irrespective if a building has a basement or a slab-on-grade foundation, the Péclet number across the foundation slab is not sufficiently high for advection to the dominant transport mechanism; most soils are too impermeable for sufficient airflow to be pulled into the building via the subsurface. Sites characterized by sand soil are an exception to this, which are permeable enough to sustain such

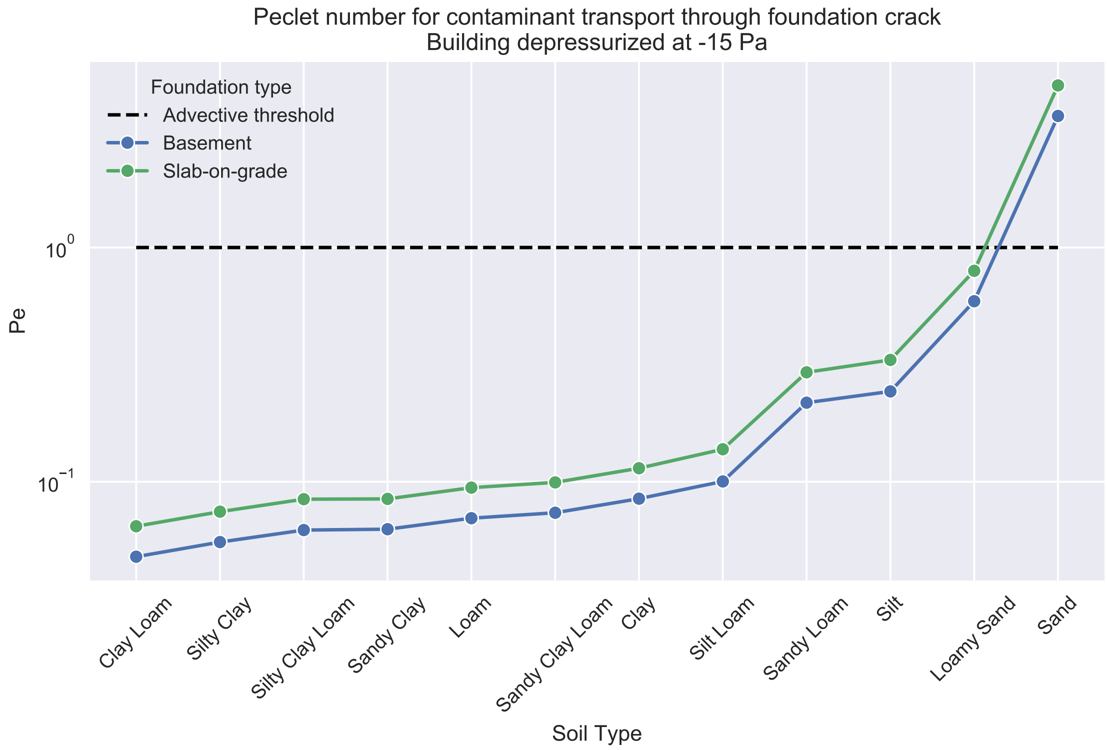

Figure 1.1: Predicted effect of soil and foundation type on the Péclet number of transport through the foundation crack. We consider the 12 different soils studied by the EPA (see Table), and for each of these we consider a house featuring a basement and a slab-on-grade house. The foundation slab is assumed to be 15 cm thick. In the basement case, the bottom of the foundation slab is assumed to be 1 m bgs and 15 cm bgs in the slab-on-grade case. The modeled building is assumed to be depressurized at -15 Pa. The threshold where advective transport begins to overtake diffusive transport, i.e $\mathrm{Pe} = 1$, is marked by the dashed line.

airflows. An example of such a site is a site at North Island Naval Air Station in San Diego, California, which featured sandy soil, and there indoor contaminant concentration and building pressurization was highly correlated[**hosangadi˙high-frequency˙2017**].

This indicates that for many sites characterized by other soil types, significant advective transport of contaminant vapors into the building are likely to occur through some preferential air source. It is important to note however, that this is not limited to the sort of preferential pathways we have studied in this work, but such a phenomena could conceivably arise from a wide range of circumstances.

1.3 Applying Transport Classification Concept

Considering if contaminant transport from the subsurface into the a building is dominated by advection or diffusion as it dramatically changes how a structure is expected to respond to change in pressurization; for diffusion dominated sites, contaminant entry rates will be relatively decoupled from building pressurization. This has implications for a wide variety of VI topics, but perhaps most relevant for using CPM and choosing relevant ITS.

1.3.1 Controlled Pressure Method

The idea of CPM is to control the building pressurization, e.g. by using some fans or blowers, which in turn will control the contaminant entry rate. The underlying assumption in its application is that contaminant entry into a building is largely advective in nature; for "diffusion sites" this will not be as effective.

Figure 1.2 illustrates this phenomena. During the period when the land drain preferential pathway was open, CPM dramatically increased indoor contaminant concentrations compared to the when the CPM system was inactive. However, after the closing of the land drain preferential pathway, CPM did not have any significant effect on indoor contaminant concentrations. From the study of the ASU house and associated modeling explained it was deduced that the presence of the land drain preferential pathway make advection the dominant transport mechanism of contaminant vapors into the building. This shows that CPM may not be universally effective, but could only reasonably expected to be so at "advection sites".

CPM not only affects the contaminant vapor entry rate into a building, but will also have an impact on air exchange rates. Figure 1.3 shows the effect that CPM had on air exchange rates at the ASU house, where they increased significantly during the period. The effect of this is that contaminant expulsion from the house is amplified, which decreases the indoor contaminant concentration for a given contaminant entry rate. This is a concern voiced in [**holton˙long-term˙2015**][**holton˙long-term˙2015**] evaluation of the CPM system at the ASU house, and suggested that a tracer-gas

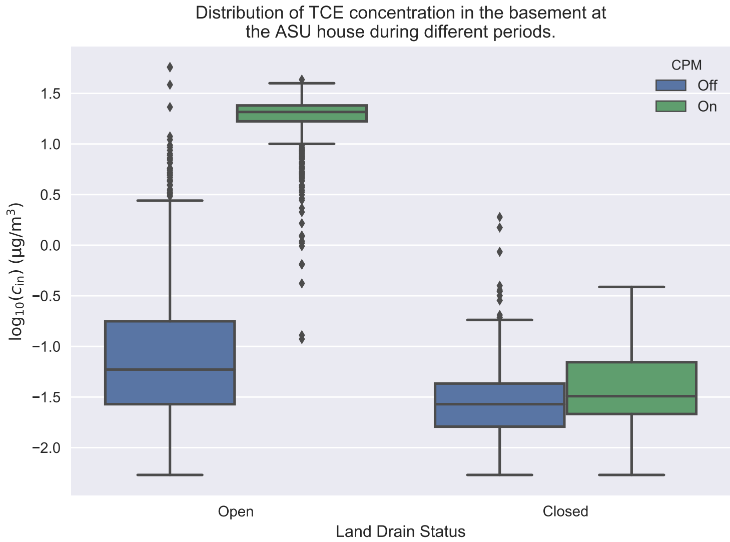

Figure 1.2: Boxplot showing the log-10 transformed TCE concentrations at the ASU house. The CPM and natural periods, and the period before and after the land drain was closed are considered separately. The box signifies the interquartile range (IQR) of values, with the central line representing the median value, and the top and bottom of the box are the 25th and 75th percentiles. The whiskers extend to 1.5 times the IQR. Markers indicate outlier data points that fall outside the whiskers.

test to measure air exchange rate should be conducted during CPM. This is used to introduce a correction term to account for the elevation of air exchange rate above its "natural" values. Since CPM is used to determine the worst-case scenario, this correction term should be used to calculate the indoor contaminant concentration with worst-case entry rates, but "natural" air exchange rate values, i.e. $\approx 0.5\,\mathrm{h}^{-1}$ instead of the elevated values.

This highlights an issue with CPM at VI sites characterized by diffusive transport. If the increased depressurization doesn't yield higher contaminant entry rates into the building, but elevates air exchange rate, then indoor contaminant concentration may be artificially lowered, and thus underdetermining the VI risk. This further shows the necessity of using tracer-gas monitoring to measure air exchange rates when using CPM.

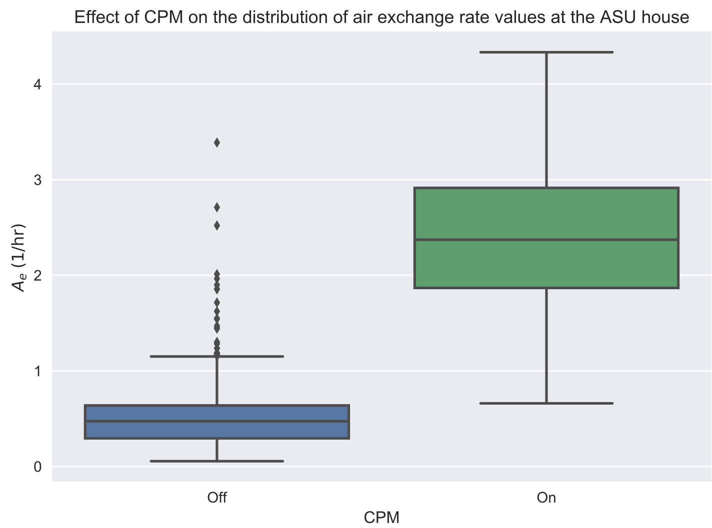

Figure 1.3: Boxplot showing the distribution of air exchange rate values at the ASU house, considering the effect of CPM.

1.3.2 Indicators, Tracers, And Surrogates

As has been discussed throughout this work, VI can feature great temporal variability in indoor contaminant concentrations. These variations can occur on a variety of time-scales, from days to larger seasonal trends, which can require significant amounts of data collection to fully resolve. To reduce the resources expended on these efforts, and increase the likelihood of determining the relevant VI risk, it is desirable to use some indicators, tracers, and surrogates (ITS) that can be used to readily predict the periods and conditions when the highest indoor contaminant concentration at a site are likely to manifest. Which specific ITS that are most appropriate for this task, and under which circumstances, are yet to be determined.

Seasonal trends have been found to be common at many VI sites, with winter often cited as the period most likely to feature elevated indoor contaminant concentrations[**burke˙estimation˙2010**, **hers˙evaluation˙2014**, **miles˙temporal˙2001**, **schumacher˙fluctuation˙2012**, **steck˙indoor˙2004**]. This is a trend that partly occurred at the ASU house as well (see Figure 1.4); indoor contaminant concentrations were highest during winter when the land drain preferential pathway was open, a trend was non-existent after the closing of the land drain. At the EPA duplex,

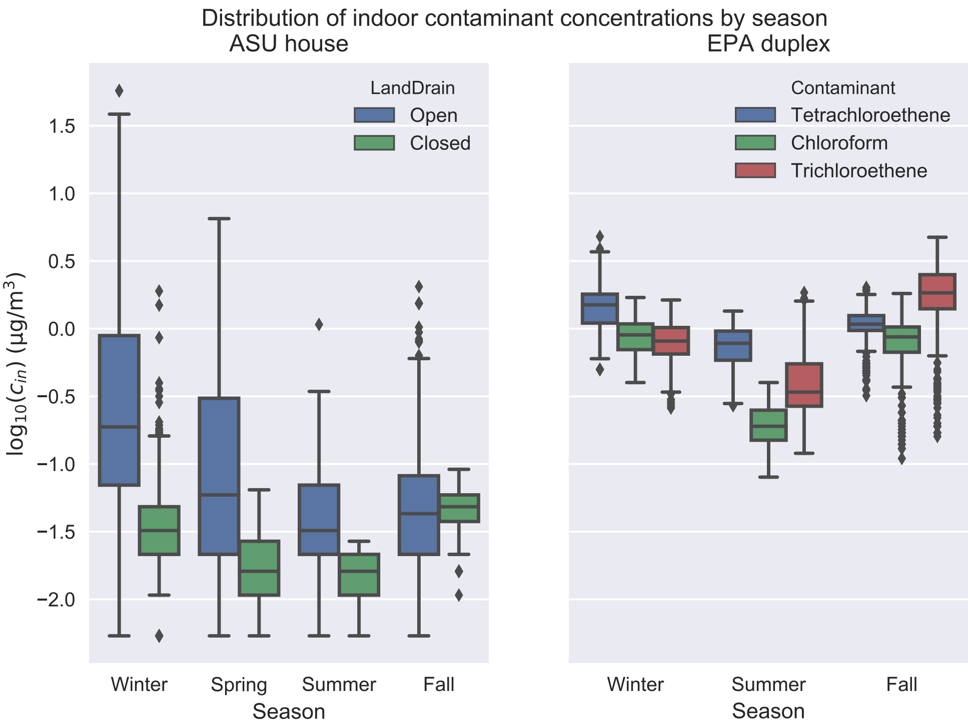

Figure 1.4: Seasonal distribution of indoor contaminant concentration at the ASU house and EPA duplex. At the ASU house, the effect of the land drain preferential pathway is considered. At the EPA duplex, the differences in distribution for three different contaminants are considered. Here ”winter” includes December to February, with each subsequent season being defined by the subsequent three months.

indoor contaminant concentrations were slightly higher during winter and fall than Summer, but only marginally so.

The seasonal trend at the ASU house when the land drain preferential pathway was open, and its disappearance can be understood by examining the seasonal distribution of indoor/outdoor pressure difference values, in Figure 1.5. Here we see that building depressurization is greatest during winter, slightly less depressurized during the shoulder seasons, and usually overpressurized during summer. Putting this together with advective transport dominated period when the land drain preferential pathway was open at the ASU house, explains why indoor contaminant concentrations are higher during the colder seasons. Conversely, when the land drain preferential pathway, contaminant transport was likely diffusion dominated, and such a trend disappears.

The EPA duplex exhibit a similar trend in building pressurization by season, i.e.

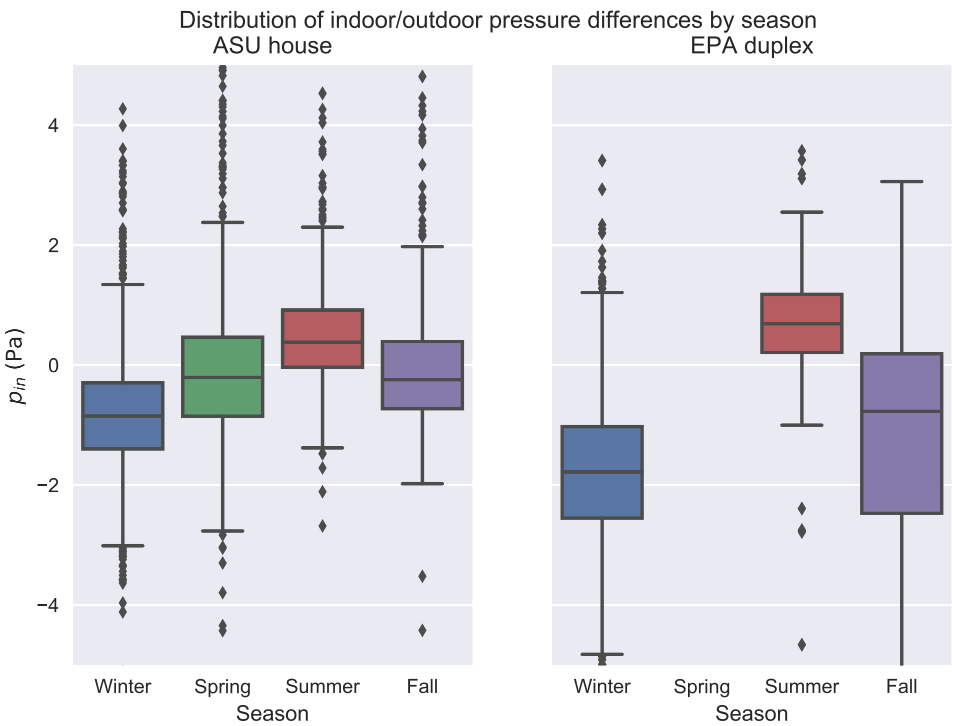

Figure 1.5: Seasonal distribution of indoor contaminant concentration at the ASU house. A negative value indicates that the building is depressurized relative to ambient.

it is more depressurized during colder seasons, and can help explain why indoor contaminant concentrations were likewise slightly higher during these seasons. While the nature of the contaminant transport into the EPA duplex is not as well understood, it was showed in Chapter ?? that association between building pressurization and indoor contaminant concentrations were somewhere between that of the ASU house before and after the closing of the land drain (compare Figures ?? and ??), indicating that while advection may not be dominant, it certainly isn't insignificant.

These data and analysis demonstrate that for advection sites, building pressurization could be used as an effective ITS, whereas at a diffusion site, it may not be. However, to use building pressurization effectively as an ITS, it would be useful to be able to predict it based on some easier to measure parameters - such as weather conditions.

1.4 Predicting Building Pressurization

Building pressurization can be used as an effective ITS under the right circumstances. However, determining this requires a measurement device to be installed, and moreover needs to record over some length of time to determine trends. Thus, it would be desirable to use some more readily available metric, such as weather data, to predict building pressurization.

A variety of factors can contribute to determine overall building pressurization. Some of these are artificially controlled and induced, such as the force convection by heating, ventilation, and air conditioning systems. These are of course difficult to use to for prediction purposes, and can at some sites be the dominant means for controlling building pressurization, i.e. some buildings or rooms are forcefully pressurized to keep gases or contamination out.

Weather primarily contributes to building pressurization through two means. The temperature difference between the interior of the building produces a density and subsequent pressure gradient on either side of the building wall - this is commonly called the *stack effect*. Wind striking the building also produces a pressure difference, the magnitude of which is largely dependent on wind speed. However, if the building is pressurized or depressurized by this, is more complicated and generally depends on the wind direction and building characteristics; wind blowing on a leaky window causes a very different effect compared to a featureless wall.

These weather phenomena likewise can affect air exchange rates, and has been a significant focus in the VI modeling work by **shirazi˙three-dimensional˙2017**[**shirazi˙three-dimensio**
As their work shows, predicting air exchange rate can be challenging, as accurate characterization often require detailed knowledge of the interior of a building, and will not be a focus in this work.

1.4.1 Wind Effects

To truly capture the impact that wind can have on a building and its pressurization, it is usually necessary to conduct wind tunnel tests of scale models of the building, or through detailed computational fluid dynamics simulations. This is especially true for buildings of even modest complex geometric shapes, where it is impossible to predict the wind pressure field without these tools. However, it is possible to derive some simple equations to account for wind effects on simple rectangular block-type buildings.

Even with assumption, the inherent turbulent nature of wind means that is truly never at steady-state, and thus wind striking a wall generates a distribution of pressures across the surface, that can vary widely across time; this requires significant computational effort to resolve accurately. However, by considering the wind induced pressure field over some time-averaged period, it is possible to develop some simple equations for predicting wind induced pressurization for a rectangular building. The drawback of this approach is that large pressure fluctuations are usually missed.

Wind is also inherently turbulent, and as such it is never truly at steady-state. Thus, wind pressure as it strikes the wall of a building can fluctuate wildly

With these limitations in mind, we introduce some equations for estimating wind induced building pressurization.

As the wind strikes the wall of a house, its velocity falls to zero, and the change in momentum is directly proportional to the change in pressure:

$$\Delta P = \frac{1}{2}\rho_{\text{air}}u_{\text{wind}}^2 \tag{1.1}$$

where $\Delta P = P_{\text{wall}} - P_{\text{wind}}$ [Pa] is the change in pressure at the building wall from the wind free-stream pressure; ρ_{air} [$\text{kg}\,\text{m}^{-3}$] is the air density; and u_{wind} [$\text{m}\,\text{s}^{-1}$] is the free-stream wind speed.

However, (1.1) neglects a variety of factors, such as the obstacles in front of the surface (e.g. vegetation or other buildings), or wind striking the surface at an angle. These can be accounted for by introducing a drag or pressure coefficient C_p, which is, using the same notation as in (1.1), defined as:

$$C_p = \frac{\Delta P}{\frac{1}{2}\rho u_{\text{wind}}^2} \tag{1.2}$$

C_p values are usually determined empirically in wind tunnel tests, or by solving the Navier-Stokes equation in some computational fluid dynamics simulation.

Introducing the C_p correction then gives

$$\Delta P = C_p \frac{1}{2}\rho_{\text{air}} u_{\text{wind}}^2 \tag{1.3}$$

1.4.2 Temperature Effects

The pressure of any fluid under the influence of gravity varies with elevation and the density of the fluid determines the magnitude of this pressure. Air is a compressible fluid and its density depends on its temperature. Therefore, if you separate two air masses between a wall, with each at a difference temperature, a pressure difference across the wall be induced, i.e. the *stack effect*.

Assuming the ideal gas law applies and that the temperature on either side is constant then

$$P = P_0 \exp\left(\frac{-M_{\text{air}} g z}{RT}\right) \tag{1.4}$$

determines the pressure variation across the wall. Where P is the pressure; P_0 the reference pressure ($z = 0$); M_{air} is the molar weight of air; z is the elevation; g is the acceleration due to gravity; R is the gas constant; and T is the temperature.

This can be further simplified by defining z_0 which is the height at which the pressure on both sides of the wall are equal, i.e. P_0. The pressure variation on either side can now be expressed in terms of distance from z_0, $z - z_0$. Assuming that the interior and exterior has a constant temperature of T_i and T_o respectively, the difference in pressure between the two sides along the wall is

$$\Delta P = P_0 \Big[\exp\left(\frac{-M_{\text{air}} g(z - z_0)}{RT_i}\right) - \exp\left(\frac{-M_{\text{air}} g(z - z_0)}{RT_o}\right) \Big] \tag{1.5}$$

Using that $e^{-x} = 1 - x$ for $x \ll 1$ the pressure difference can be expressed as

$$\Delta P = \alpha\Big(\frac{1}{T_o} - \frac{1}{T_i}(z - z_0)\Big) \tag{1.6}$$

where $\alpha = \frac{P_0 M_{\mathrm{air}} g}{R} \approx 34543454\,\mathrm{Pa\,K}\ \frac{\mathrm{Pa\cdot K}}{\mathrm{m}}\mathrm{Pa}$. Here a negative pressure differnece, $\Delta P < 0$, indicates an inward flow.

1.4.3 Heating, Ventilation And Air Conditioning

1.4.4 Predicting Pressurization At The EPA Duplex

The equations for predicting p_{in} as a function of temperature and wind are applied to the weather data from EPA duplex, and

	Data	3cPrediction		
		p_{temp}	$p_{\mathrm{temp}} + p_{\mathrm{wind}}$	$p_{\mathrm{temp}} + p_{\mathrm{wind,corr}}$
Mean	-1.33	-1.50	-0.83	-1.37
Std.	2.15	1.12	1.40	1.50

Table 1.1

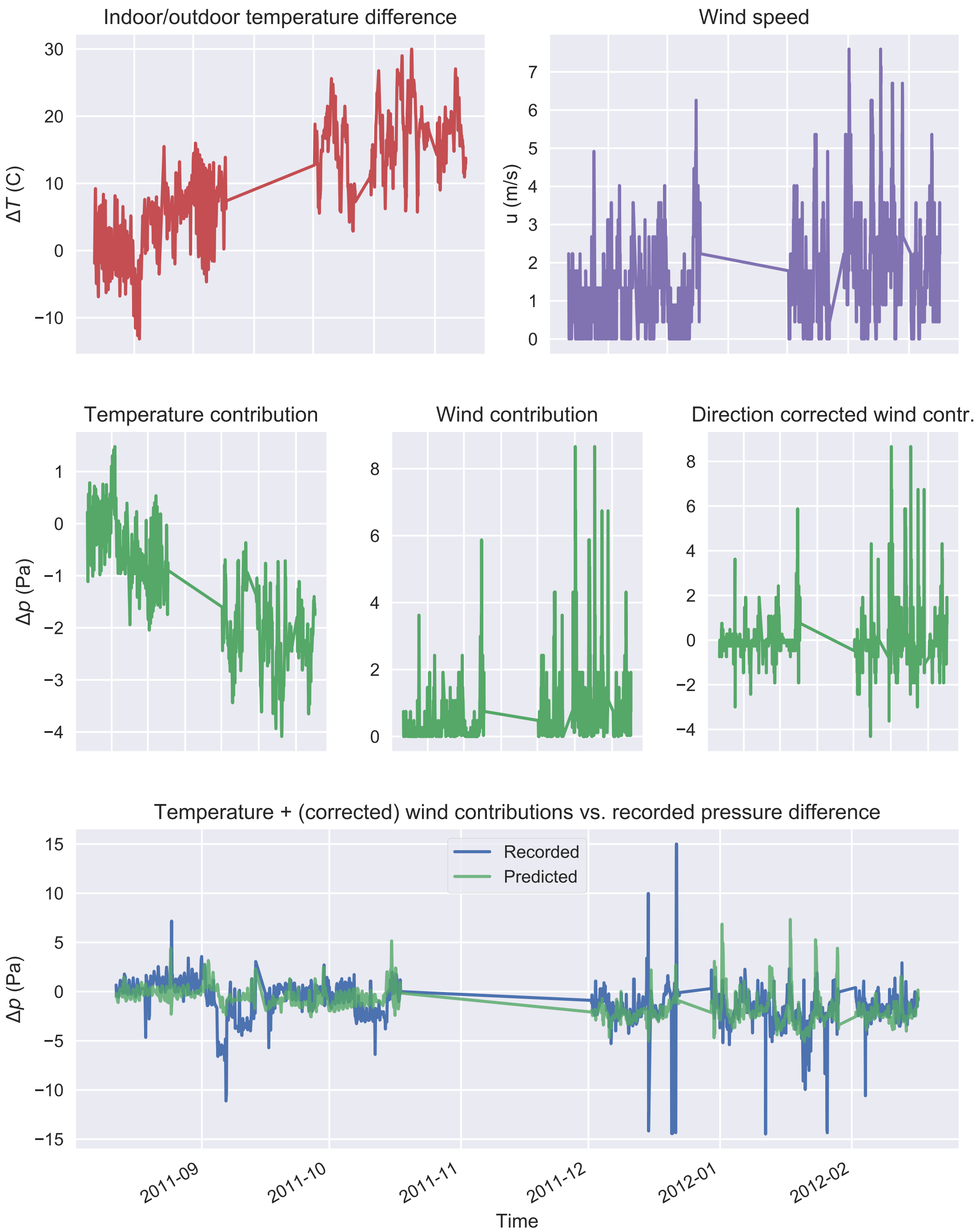

Figure 1.6: TBD